A study of dislocation transmission through a grain boundary in hcp Ti–6Al using micro-cantilevers

Rengen Ding, Jicheng Gong, Angus J. Wilkinson and Ian P. Jones

a School of Metallurgy and Materials, The University of Birmingham, Birmingham, B15 2TT, UK
b Department of Materials, University of Oxford, Oxford, OX1 3PH, UK

Copy of record is published as

Acta Materialia, (2016) Volume 103, 416–423

The paper is available at:
http://dx.doi.org/10.1016/j.actamat.2015.10.023

A study of dislocation transmission through a grain boundary in hcp Ti-6Al using micro-cantilevers

Rengen Ding[a], Jicheng Gong[b], Angus J. Wilkinson[b] and Ian P. Jones[a]

a School of Metallurgy and Materials, The University of Birmingham, Birmingham, B15 2TT, UK

b Department of Materials, University of Oxford, Oxford, OX1 3PH, UK

Abstract

Micro-cantilevers with an equilateral triangular cross-section and an apex at the bottom were machined across grain boundaries in a Ti-6Al alloy sample using a focused ion beam (FIB). A nano-indenter was used to deform the micro-cantilevers. An <a> prism slip system was selectively activated in the upper grain by controlling the crystal orientation along the micro-cantilever. Specimens for transmission electron microscopy (TEM) were prepared from the deformed micro-cantilevers using dual-beam FIB. Bright field scanning transmission electron microscopy was used to investigate the process of slip propagation through the grain boundary.

Keywords: Microcantilever; focussed ion beam; transmission electron microscopy; grain boundary; dislocation motion.

Introduction

Grain boundaries play an important role in controlling the mechanical properties of many materials. The hardening effect of boundaries in single-phase polycrystalline materials is commonly described by the proportionality factor k_y in the Hall-Petch relation

$$\sigma_y = \sigma_o + k_y d^{-1/2} \qquad (1)$$

where σ_o is a material constant representing the stress required to cause dislocation motion *within* a grain. The slope k_y measures the propensity of the grain boundaries to resist the transmission of slip and is typically determined from deformation tests on specimens with varying grain sizes, giving an average value of k_y over all the grain boundaries. Dunstan and Bushby [1] have recently re-evaluated grain size effect data and concluded that

$$\sigma_y = \sigma_o + k_y d^{-1} \qquad (2)$$

gives a better representation of data from a range of metallic systems.

As far as individual grain boundaries and individual impinging slip systems are concerned, most papers restrict themselves to a consideration of a single transmitted slip system (where here 'transmitted' can refer either to transmission from Grain 1 into Grain 2) (for example: fig. 1), or to reflection back into Grain 1. The aim has generally been to predict the most favoured transmitted slip system and to some extent how favoured it is.

Various criteria for 'most favoured' status have been suggested:

1. The shear stress acting on the transmitted system. This is a superposition of the externally applied stress and its concentration at the tip of the incoming slip system where it impinges on the grain boundary. The latter dominates close to the tip of the pile-up. For example, an expression for the shear stress on a slip system in Grain 2 assuming a pure shear stress acting on the incoming slip system in Grain 1 and acting locally on Grain 2 is given by Livingston and Chalmers [2]; it is simply the ratio of the shear stress on the incoming slip system in Grain 1 to that on the slip system in Grain 2, after axis rotation.

   The *macroscopic*, as opposed to *local*, stress (see for example Kacher et al. [3]) is sometimes referred to simply as a Schmid factor criterion.

2. There are various geometrical criteria [3-6]. For example, the angle between the two lines of intersection of, the incoming and outgoing slip system planes and the grain boundary should be a minimum (see fig. 1).
3. Any residual dislocation Burgers vector (the difference between the incoming and outgoing Burgers vectors) should be a minimum [5]. This includes, amongst other things, the angle between the Burgers vectors.
4. If the incoming or outgoing dislocation is related to the pre-existing grain boundary dislocations, this may affect transmissibility [4].

Different circumstances will affect the relative importance of criteria 1-4 above, which renders grain boundary hardening a complex phenomenon. Criteria 2 and 3 are often combined into a single scalar factor measuring the alignment of available slip systems within the neighbouring grain, for example the factor M_{Shen} proposed by Shen et al. [5,7]:

$$M_{Shen} = \frac{(\boldsymbol{L_1}.\boldsymbol{L_2})(\boldsymbol{b_{in}}.\boldsymbol{b_{out}})}{|\boldsymbol{b_{in}}||\boldsymbol{b_{out}}|} \qquad (3)$$

where $\boldsymbol{L_1}$ and $\boldsymbol{L_2}$ are unit vectors along the intersections with the grain boundary plane of the incoming and outgoing slip planes, and $\boldsymbol{b_{in}}$ and $\boldsymbol{b_{out}}$ are the Burgers vectors of the incoming and outgoing dislocations. In some studies the grain boundary plane is not well known, leading Werner and Prantl [8] to introduce the factor M_{Werner} (also used by Luster and Morris [9])

$$M_{Werner} = \frac{(\boldsymbol{n_1}.\boldsymbol{n_2})(\boldsymbol{b_{in}}.\boldsymbol{b_{out}})}{|\boldsymbol{b_{in}}||\boldsymbol{b_{out}}|} \qquad (4)$$

where $\boldsymbol{n_1}$ and $\boldsymbol{n_2}$ are unit vectors along the normals to the incoming and outgoing slip systems. Such M factors are close to their maximum value of 1 if the slip systems are well aligned and so the preferred outgoing slip system is taken to be the one that maximises M; the ease of slip transfer is also correlated to the magnitude of M.

The number of resulting slip systems was three for Livingston and Chalmers's [2] unusually unconstrained system, but more generally is five [10, 11]. The *amount* of slip on each system does not seem to have received much attention.

The methods for investigating slip transmission across grain boundaries have been reviewed by Kacher et al. [3]* and include slip trace studies accomplished using optical microscopy, scanning electron microscopy (SEM), or even atomic force microscopy (AFM) [12, 13], X-ray diffraction using synchrotron radiation [14, 15], electron backscattered diffraction (EBSD) [16, 17] and digital image correlation [18-20] and nanoindentation [21, 22]. TEM studies [3-7, 23, 24] have proved an invaluable method for revealing detailed dislocation mechanisms. Many of the investigations referred to involved meticulous experimentation and interpretation. For polycrystalline materials, however, it is quite difficult to investigate the transmission behaviour of a *defined* slip system across a *specific* grain boundary. Most TEM investigations have been *post mortem,* where the chief danger is rearrangement of the dislocations when the load is removed or, later, during specimen preparation. For *in-situ* TEM, however, there is the possibility that the free surfaces facilitate nucleation of slip in adjacent grains due to the lack of constraint and that slip bands develop following this nucleation process; a worse problem is change of slip plane.

---

* A recent issue of Current Opinion in Solid State and Materials Science (Vol. 18, Issue 4, 2014) contains several papers/reviews (two of which have been referred to here) concerning grain boundary hardening.

There are fewer reports of investigations into hcp-based polycrystals as compared to cubic, particularly face centred cubic. Britton and Wilkinson [16] and subsequently Guo et al. [17] have used EBSD strain mapping in Ti to characterise the local stress concentrations at the heads of blocked slip bands. Wang et al. [25] used surface trace analysis and EBSD, and Bieler et al. [14, 26] synchrotron based 3DXRD, to examine strain transfer by slip nucleation of twinning in Ti. A detailed TEM study has recently been reported by Kacher and Robertson [27] for commercially pure Ti deformed *in situ* and *ex situ* and including collection of some dislocation tomograms showing the full 3D nature of the dislocations generated. Kacher and Robertson [27] noted dislocation interactions *in situ* were generally simpler than in samples deformed *ex situ* where emission of multiple dislocations was more common, presumably as a result of greater constraint in the bulk samples. The work on Ti suggests that although complicated by the differing slip systems available and greater anisotropy the geometric criteria developed mostly from observation of fcc systems are still applicable.

In this work we have used FIB to make microcantilevers across grain boundaries in (hcp) Ti-6Al. The microcantilevers were deformed via a nanoindenter. Subsequently TEM specimens were FIB machined from the cantilever [28, 29] and then examined. The attractions of this method are that (i) many cantilever specimens can be machined from across the same grain boundary, thus evidencing reproducibility and (ii) different identical specimens can be strained to different extents; finally (iii) we know pretty well where the incoming dislocations will come from and in which direction they are travelling. The demerits of this method are that (i) we cannot currently observe the dislocations *in-situ* and (ii) the complexity of the stress system makes it difficult to know exactly what the stress is at any one point. We have paid particular attention to (i) *which* slip systems are activated and (ii) *how much* slip there is on each.

Experimental procedure

Samples about 10×10×3 mm^3 were cut using a low speed diamond saw from an annealed Ti-6Al block with a large grain size attained by vacuum heat treatment. One 10×10 mm^2 surface of each block was carefully ground and polished. Final polishing was performed using 0.02 μm colloidal silica for 30 minutes. EBSD was then used to identify the grain orientations and to choose a specific grain boundary. In the example used here the *c*-axes of both grains were parallel to the sample surface and nearly parallel to each other. For one grain (G1 in fig. 2a) the surface is about 15° away from the nearest prism plane (and thus about 45° away from the next prism plane); for G2 the sample surface was nearly parallel to a prism plane. Cantilevers were prepared as shown in fig. 2 to be 30 μm long and 5 μm wide with an equilateral triangular cross-section and one apex at the bottom of the cantilever. Cantilevers were cut wholly within each of the individual grains G1 and G2, while others contained the targeted grain boundary which was located nearly at the built-in end of the cantilever (fig. 2). Micro-bending tests were performed using a NanoXP nanoindentation system. The deflection rate at the free end was 10 nm/s which corresponds to a maximum strain rate of 2.5×10^{-4}/s at the bottom edge of the cantilever at its built-in end. Since the long axis (LA) of the cantilever is perpendicular to the *c* axes of both grains, only prismatic slip systems would be activated for both grains and single slip (on the prismatic slip plane 45° away from the surface of the cantilever) is expected to be activated for G1. Thus this is almost a 2-D problem: the incoming prismatic slip system in G1 might be expected to give rise to two transmitted prismatic slip systems in G2.

TEM foils were prepared along the LA of the cantilever by focussed ion beam milling in an FEI Quanta 3D FIB. The TEM foil normal is thus nearly parallel to the *c*-axis in both grains. The initial stages of foil preparation involved a 30 keV ion beam; the probe current was

reduced successively throughout the procedure and final polishing/cleaning was performed at 5 keV. Then an *in-situ* micromanipulator (OmniProbe^{TM}) was used to extract the membrane, with the Omniprobe was attached to the matrix away from the cantilever in order to avoid extra deformation of the deformed region of the cantilever during the lift-out.

TEM samples were examined in an FEI Tecnai F20. The dislocation Burgers vectors were analysed using the standard $\mathbf{g}\cdot\mathbf{b} = 0 \Rightarrow$ invisibility criterion. Upon examination of the TEM samples, it was found that bending of the foils caused problems for conventional diffraction contrast imaging, especially when trying to image entire sections. Bright-field scanning TEM (BF-STEM) imaging was used to minimize these effects, as in our previous studies of Ti-6Al-4V micro-cantilevers [28, 29].

Results

Example load-displacement data from the bend tests on micro-cantilevers cut into the two individual grains and the bi-crystal are shown in fig. 3a. The softest micro-cantilever is the G1 single crystal which has the higher Schmid factor of 0.5 and the load-displacement data are in good agreement with previous tests on this material [30]. Load drops such as that seen at a displacement of ~2750 nm for micro-cantilever G1 have been previously reported in this material [30] and are commonly seen in small scale mechanical testing due to the large strains that can be generated by activation of a single dislocation source or removal of a particular dislocation obstacle. Larger loads are required to deform the G2 single crystal but the increased strength is well accounted for by the lower Schmid factor (~0.47). For the bi-crystal the softer G1 crystal forms the upper part of the micro-cantilever at the built-in end and so experiences a lower strain and stress than the lower part of the beam, due to the triangular cross-section. Yielding typically occurs at a rather low displacement while the load-displacement curve still appears to be quite linear due to the relatively small volume

within the initial plastic zone at the apex on the lower side of the beam at the built-in end [28]. Crystal plasticity finite element analysis (CP-FEA) indicates that plasticity begins at a displacement of ~800nm and that the plastic zone spreads significantly along the length of the cantilever as deformation continues and also into its thickness but never sufficiently to impinge on the grain boundary. From a displacement of ~1500nm CP-FEA suggests deformation is also nucleated on the top side of the cantilever near the built-in end. The tensile plastic zone occupies a markedly larger material volume and thus has a marked impact on the load-displacement curve which begins to show obvious non-linearity. The level at which the load tends to plateau is thus strongly influenced by the upper region of the micro-cantilever and so the bi-crystal response is rather closer to that of the softer G1 single crystal case. By an end point displacement of 4000nm for the bi-crystal micro-cantilever the plastic strain along the cantilever axis is rather larger in the top part (soft grain G1) than it was in either of the single crystal micro-cantilevers (see fig 3b), while in the lower part the compressive strains are smaller in the bi-crystal (harder grain G2) than in the single crystal cases.

Figure 4 shows SEM images of the cantilevers deflected by 2.8 μm (fig. 4a) and 4.0 μm (fig. 4b) at the load point. The cantilever samples were tilted by 52° about the long axis of the cantilever to reveal both the top and side surfaces. The SEM image of the 2.8 μm deflected cantilever shows slip traces at the top and side surfaces of the cantilever (fig. 4a). The slip traces are deviated at the grain boundary, as shown in the inset to fig. 4a. When the sample was deflected by 4.0 μm, more slip traces were observed on both the top and side surfaces, as shown in fig. 4b. For example, there are 3 clear slip traces (arrowed) on the top surface of G1 while there are 2 clear slip traces (arrowed) on the visible side of G1. There is also a slip trace (arrowed) in G2 towards the bottom of the cantilever (fig. 4b).

TEM foils were cut along the LA (the white line in fig. 4b) by FIB. A montage of BF-STEM images is shown in fig. 5a (2.8 μm deflection) and fig. 5b (4.0 μm deflection), which show clearly 1 slip band in G1 for the 2.8 μm and 3 slip bands in G1 for the 4 μm deflected samples. These slip bands correspond to slip traces on the top surfaces (fig. 4). The position of the first slip band is identical in figs 4a and b and intersects the top surface where it, in its turn, intersects the bulk material at the built-in end of the cantilever. The maximum compressive stress at the bottom edge of the cantilever is twice the maximum tensile stress at the top. Clearly in fig. 5a there is considerable dislocation activity at the bottom of the cantilever, but little at the top, barring the single slip plane coming down from the intersection of the cantilever and the bulk at the built-in end. Slip along the lower edge of G2 is divided between $a_2^{(2)}$ and $a_1^{(2)}$ dislocations and is spread 7-8μm along the length of the cantilever. Although the CP-FEA simulation does not capture the discrete slip bands that can be seen in fig. 5a, the general shape of the plastic zone is in good agreement, as is the activation of the two prism slip systems (fig. 3b). Apart from the slip activity below the ledge in the grain boundary there are one or two $a_2^{(2)}$ dislocations (subscript: Burgers vector a_1, a_2 *or* a_3; superscript G1 or G2) which have travelled up from the bottom to be within ~1μm of the grain boundary. (The angles between the slip traces are not exactly 60˚ or 120˚ because the electron beam direction is not exactly [0001].)

The grain boundary

Diffraction was used to analyse the character of the grain boundary. Convergent beam electron diffraction patterns (CBED) from G1 and G2 in the 4.0 μm deflection TEM specimen are shown in fig. 6a and 6b; fig. 6c is a composite selected area diffraction (SAD) pattern across the grain boundary. CBED and SAD confirm that the normals to the two grains are close to [0001] (to be more precise, here, $[2\,\bar{1}\,\bar{1}\,14]$). There is a rotation of 19˚ about 0001 (or $[2\,\bar{1}\,\bar{1}\,14]$). The diffraction analysis shows that the grain boundary plane is $(\bar{2}3\bar{1}0)$

referred to G1 and $(3\bar{8}50)$ referred to G2. The grain boundary is thus essentially a tilt boundary with the rotation axis within the boundary plane. The geometry is such that the angle between L_1 and L_2 in fig. 1 is negligibly small for the $a_2^{(1)}$ to $a_2^{(2)}$ slip transfer so that only the misalignment of slip directions contributes to the M_{Shen} factor which is very high at ~0.95. The M_{Werner} factor (which is always smaller than M_{Shen}) is ~0.9.

The slip systems

There is 1 plastic deformation event associated with the grain boundary in fig. 5a and 3 similar events in fig. 5b. Those features of the plastic deformation which are reproduced at both deflections and at different places on the grain boundaries are shown schematically in fig. 7. There are five separate aspects to each reaction: (i) the incoming slip system $a_2^{(1)}$, (ii) the reflected slip systems $a_1^{(1)}$ and $a_3^{(1)}$, (iii) the transmitted slip systems $a_2^{(2)}$ and $a_3^{(2)}$, (iv) the ledge introduced to the grain boundary and, finally, (v) slip along the grain boundary.

(i) The incoming slip system $a_2^{(1)}$

This system constitutes the *incoming* slip dislocations because (a) the Schmid factor is largest for this system (see table 1) and (b) the neutral (zero stress) line passes close to one example of the grain boundary reaction, so nucleation close to or at the boundary is unlikely as the stress is very low. The Burgers vector of the dislocations was confirmed to be a_2. For a deflection of 4 μm the sizes of the steps at the top surface are 37, 32 and 35 nm (left to right). These correspond roughly to 125, 108 and 118 dislocations for a Burgers vector of 0.295 nm. For slip band 1, for example, there are at least 20 dislocations remaining in the slip plane (see table 2).

(ii) The reflected slip systems $a_1^{(1)}$ and $a_3^{(1)}$

The prismatic slip planes are evident from figs 5a and 5b. The Burgers vectors were confirmed to be a_1 and a_3. For a deflection of 4 μm the numbers of dislocations in slip band 1 were estimated as 17 ($a_1^{(1)}$) and 19 ($a_3^{(1)}$) (see table 2).

(iii) The transmitted slip systems $a_2^{(2)}$ and $a_3^{(2)}$

The prismatic slip planes are evident from fig. 5. The Burgers vectors were confirmed to be a_2 and a_3. For a deflection of 4 μm the numbers of dislocations in slip band 1 were estimated as ~50 ($a_2^{(2)}$) and 17 ($a_3^{(2)}$) (see table 2).

(iv) The ledge introduced to the grain boundary

The sense of the ledges both at the grain boundary and at the top of the cantilever is consistent with a tensile stress at the top of the cantilever. Fig. 8a demonstrates that for a deflection of 4 μm the plane of the arrowed facet 1 is ~$(3\bar{2}\bar{1}0)$ referred to G2 and that its length is 21 nm. Facet 2 is 23 nm long and lies on ~$(1\bar{1}00)$ in G2. Facet 3 (fig. 8b) does not constitute a discrete step and has a long jagged tail.

(v) Slip along the grain boundary

Fig. 9 shows micrographs of the grain boundary at its intersection with a slip band. Grain boundary dislocations can be seen, but the quality of the TEM specimen did not permit their Burgers vectors to be identified unambiguously. Without knowledge of the dislocation content before deformation it is not possible to say whether or not the grain boundary has slid.

Analysis

Fig. 7 shows that in response to the incoming $a_2^{(1)}$ dislocations there are 6 shear mechanisms: the reflected dislocations $a_1^{(1)}$ and $a_3^{(1)}$, the transmitted dislocations ($a_2^{(2)}$) and ($a_3^{(2)}$) and shear in either direction on the grain boundary. Any of the three pairs of shears, in differing combinations, could absorb the incoming shear. The grain boundary facet is not a shear mechanism as such, but its plane and magnitude reflect the balance between the six shear responses. The individual shears are not independent of one another. We know fairly exactly the magnitude of the incoming shear, the numbers of dislocations in the reflected slip systems and those in the transmitted slip systems. We do not know, for reasons outlined above, the numbers of grain boundary dislocations moving in either directions, nor their Burgers vectors. We do know, however, the size and plane of the grain boundary facet. All this information, where it was accessible, is contained in table 2.

In the specific situation we have investigated here, the two grains, G1 and G2, are rotated about [0001] by 19˚ and the grain boundary itself is nearly parallel to [0001]. All the prismatic slip planes have in common [0001] as a zone axis. This is thus almost a 2-D situation. Referring back to fig. 1, it is difficult to imagine a situation leading to easier dislocation transmission, whatever happens to be the controlling criterion. In particular, there should be no or few residual dislocations left in the grain boundary. It should be noted that we are explicitly allowing more than one transmitted (and reflected) slip system (as indeed is observed), unlike most analyses in the literature.

And yet, there are still reflected dislocations. For slip band 1 (for example) there are 17 $a_1^{(1)}$ reflected dislocations and 19 $a_3^{(1)}$ reflected dislocations. The two populations for facets 2 and 3 are slightly more different, but not grossly so. The total magnitude of the reflected shear is fairly constant. This all suggests a fairly uncomplicated process for reflection.

The planes of the facets reflect a balance between the shears associated with the grain boundary shears and the transmitted shears, resolved onto the grain boundary. Interestingly, although the magnitude and nature of the reflected and transmitted slip are fairly similar for facets 1-3 (4 μm deflection), the one feature which does vary is the plane of each facet. The grain boundary is gently curved, as shown in fig. 2, so the nature of the pre-existing grain boundary dislocations will change. This could cause to change the grain boundary slip characteristics. Certainly for facet 3 (see fig. 8b) the exact sites of the dislocation reflection and transmission appear to be spread along the grain boundary. In principle, parts of this ledge (or 'disconnection') could be migrating along the grain boundary [31], although the debris in the neighbouring grains (especially visible in G2 in fig. 8b) suggests this is not the case in any simple sense. Certainly the processes of reflection and grain boundary sliding may well be intimately connected with, if not controlled by, disconnection behaviour under stress.

Assuming that the grain boundary dislocation Burgers vectors lie in the boundary, the *sizes* of the facets normal to the grain boundary should correspond to the sum of the transmitted Burgers vectors resolved onto the same direction. Referring again to fig. 7 and to table 2, for slip band 1, for example, the size of the facet normal to the grain boundary is 17.6 nm (21× sin 57°), which is in agreement with 17.7 nm = (cos52° ×17 + cos8°×50)× 0.295 nm, which is the sum of the transmitted Burgers vectors resolved onto the same direction.

Finally, some book-keeping. The ledges at the top of the cantilever should correspond to the total shear observed. Slip step 1 at the top corresponds to 125 dislocations (see table 2). 20 $a_2^{(1)}$ are retained (maybe plus one or two in the boundary). $(17 + 19)\, cos60^{\circ} = 18$ are reflected. 50 $a_2^{(2)}$ dislocations and 17 $a_3^{(2)}$ dislocations imply that an equivalent of 60 $a_2^{(1)}$ (= 50cos19° + 17cos41°) are transmitted. $125 \rightarrow 20 + 18 + 60 = 98$. There is, therefore,

some scope for slip along the grain boundary. Thus for facet 1, in terms of equivalent dislocations on $a_2^{(1)}$, 125 dislocations → ~60 transmitted dislocations, ~20 reflected dislocations and perhaps ~25 grain boundary dislocations. Whether there is a reflected slip system or grain boundary slip presumably depends on the adhesive and shear strengths, respectively, of this grain boundary.

This was a happy, if somewhat serendipitous, choice of boundary because it was so simple. As regards further work using this micro-cantilever method, many more experiments suggest themselves: variation of the five degrees of freedom of the grain boundary (preferably one by one), change of strain rate and of temperature, different crystal structure etc. etc..

Our original intention in this project was to measure k_y in the Hall-Petch expression (equation 1) for individual boundaries. Two factors are against this: (i) the stress varies rapidly across the cantilever, even accepting it can be modelled to some extent and (ii) although the creation of a new slip band at the top surface can sometimes be identified on the load-displacement curve, we have never confidently identified a grain boundary transmission event on the stress-strain curve. This is an easy-transmission grain boundary, however – recall that the whole reaction is present and complete at low stresses (see fig. 5b). A more difficult or opaque grain boundary might leave a more observable signature on the load-displacement curve. The slip plane alignment factors of $M_{Shen} = 0.95$ and $M_{Werner} = 0.9$ and the relatively high Schmid factor (0.47) on the outgoing $a_2^{(2)}$ slip system would be place this particular boundary in a category for which Guo et al. [17] found no stress concentration at the grain boundary, but obvious slip transfer.

Kacher and Robertson [27] noted that slip transfer events observed during in situ deformation of thin TEM foils tended to produce a single emitted dislocation type while foils extracted from bulk deformed samples showed more complex interactions involving multiple systems.

The observation here of multiple transmitted and reflected slip systems indicates that the micro-cantilevers are sufficiently thick to capture bulk-like behaviour.

There has been some recent activity in using computational approaches to examine slip transfer at the atomistic level. As noted in the recent review by Spearot and Sangid [32] this has mostly been targeted at cubic systems (particularly fcc) and higher symmetry, low-Σ coincident site lattice boundaries. It is hoped that observations such as those presented here and by Kacher & Robertson [27] will encourage computational analysis of dislocation grain boundary interactions in hcp crystals. In general simulations tend to consider only a single (or small number <10) of incoming dislocations and do not predict the complex interaction observed here with multiple transmitted and reflected systems being activated.

Conclusions

The micro-cantilever method of examining grain boundaries is capable of yielding valuable information, especially when augmented by post mortem TEM analysis. Quantitative stress-strain data obtained from small regions at targeted grain boundaries can then be linked directly to the dislocation processes that have taken place during the grain boundary interaction. The analysis of slip step heights and numbers of dislocations of each Burgers vectors remaining in the foil afforded by the micro-cantilever structure allows a quantitative geometric analysis of the expected displacement at the grain boundary. This level of quantification for grain boundary ledge formation and grain boundary sliding is an attractive feature of this approach.

Acknowledgements

This work was funded by the Engineering and Physical Sciences Research Council (EPSRC) via grants EP/E044514/1 and EP/E044778/1. We thank Professor John Knott and Dr. Y.Chiu

for some early comments, Professors Bob Pond and Ian Robertson for reviewing the paper and Prof. David Rugg (Rolls-Royce) for his interest throughout the project.

References

[1] D.J. Dunstan and A.J. Bushby, Grain size dependence of the strength of metals: The Hall-Petch effect does not scale as the inverse square root of grain, Inter. J. Plasticity. 53 (2014) 56-65.

[2] J.D. Livingston and B. Chalmers, Multiple slip in bicrystal deformation, Acta Metall. 5 (1957) 322-327.

[3] J. Kacher, B.P. Eftink, B. Cui and I.M. Robertson, Dislocation interactions with grain boundaries, Current Opinion in Solid State and Materials Science. 18 (2014) 227-243.

[4] T.A. Bamford, B. Hardiman, Z. Shen, W.A.T. Clark and R.H. Wagoner, Micromechanism of slip propagation through a high angle boundary in alpha brass, Scripta Met. 20 (1986) 253-258.

[5] Z. Shen, R.H. Wagoner and W.A.T. Clark, Dislocation pile-up and grain boundary interactions in 304 stainless steel, Scripta Met. 20 (1986) 921-926.

[6] T.C. Lee, I.M. Robertson and H.K. Birnbaum, Prediction of slip transfer mechanisms across grain boundaries, Scripta Met. 23 (1989) 799-803.

[7] Z. Shen, R.H. Wagoner and W.A.T. Clark, Dislocation and grain boundary interactions in metals, Acta Metall. 36 (1988) 3231-3242.

[8] E. Werner and W. Prantl, Slip transfer across grain and phase boundaries, Acta Metall. 38 (1990) 533-537.

[9] J. Luster and J.M. Morris, Compatibility of deformation in two-phase Ti-Al alloys: Dependence on microstructure and orientation relationships, Metall. Mater. Trans. A, 26 (1995) 1745.

[10] G.I. Taylor, Plastic strain in metals, J. Inst. Met. 62 (1938) 307-324.

[11] J.F.W. Bishop and R. Hill, A theoretical derivation of the plastic properties of a polycrystalline face-centered metal, Phil. Mag. 42 (1951) 1298-1307.

[12] E.A. West and G.S. Was, A model for the normal stress dependence of interganular cracking of irradiated 316L stainless steel in supercritical water, J Nucl. Mater. 408 (2011) 142-152.

[13] Y. Yang, L. Wang, T. Bieler, P. Eisenlohr and M. Crimp, Quantitative atomic force microscopy characterization and crystal plasticity finite element modelling of heterogeneous deformation in commercial purity titanium, Metall. Mater. Trans. A 42 (2011) 636-644.

[14] T.R. Bieler, L. Wang, A.J. Beaudoin, P. Kenesei, U. Lienert, In situ characterization of twin nucleation in pure Ti using 3D-XRD, Metall. Mater. Trans. A 45 (2014) 109-122.

[15] Y. Guo, D.M. Collins, E. Tarleton, F. Hofmann, J. Tischler, W. Liu, R. Xu, A.J. Wilkinson and T.B. Britton, Acta Mater. 96 (2015) 229-236.
[16] T.B. Britton and A.J. Wilkinson, Stress fields and geometrically necessary dislocation density distributions near the head of blocked slip band, Acta Mater. 60 (2012) 5773-5782.
[17] Y Guo, T.B. Britton and A.J. Wilkinson, Slip band-grain boundary interactions in commercial –purity titanium, Acta Mater. 76 (2014) 1-12.
[18] W.Z. Abuzaid, M.D. Sangid, J.D. Carroll, H. Sehitoglu and J. Lambros, Slip transfer and plastic strain accumulation across grain boundaries in Hastelloy X, J Mech. Phys. Sols. 60 (2012) 1201-1220.
[19] L. Patriarca, W. Abuzaid, H. Sehitoglu, H.J. Maier, Slip transmission in bcc FeCr polycrystal, Mater. Sci. Eng. A 588 (2013) 308-317.
[20] M.D. McMurtrey, G.S. Was, B. Cui, I. Robertson, L. Smith, D. Farkas, Strain localization at dislocation channel-grain boundary interactions in irradiated stainless steel, Int. J. Plast. 56 (2014) 219-231.
[21] M.G. Wang and A.H.W. Ngan, Indentation strain burst phenomenon induced by grain boundaries in niobium, J. Mater. Res. 19 (2004) 2478-2486.
[22] T.B. Britton, D. Randman and A.J. Wilkinson, Nanoindentation study of slip transfer phenomenon at grain boundaries, J. Mater. Res. 24 (2009) 607-615.
[23] I.M. Robertson, T.C. Lee and H.K. Birnbaum, Application of the in situ TEM deformation technique to observe how 'clean' and doped grain boundaries respond to local stress concentrations, Ultramicroscopy. 40 (1992) 330-338.
[24] T. Ohmura, A.M. Minor, E.A. Stach and J.W. Morris, Jr., Dislocation-grain boundary interactions in martensitic steel observed through in situ nanoindentation in a TEM, J. Mater. Res. 19 (2004) 3626-3632.
[25] L. Wang, Y. Yang, P. Eisenlohr, T.R. Bieler, M.A. Crimp, D.E. Mason, Twin nucleation by slip transfer across grain boundaries in commercial purity titanium, Metall. Mater. Trans. A. 41 (2010) 421-430.
[26] T.R. Bieler, P. Eisenlohr, C. Zhang, H.J. Phukan and M.A. Crimp, Grain boundaries and interfaces in slip transfer, Current Opinion in Solid State and Materials Science. 18 (2014) 212-226.
[27] J. Kacher and I.M. Robertson, In situ and tomographic analysis of dislocation / grain boundary interactions in α-titanium, Phil Mag. 94 (2014) 814-829.
[28] R. Ding, J.C. Gong, A.J. Wilkinson and I.P. Jones, Transmission electron microscopy of deformed Ti-6Al-4V micro-cantilevers, Phil. Mag. 92 (2012) 3290-3314.

[29] R. Ding, J.C. Gong, A.J. Wilkinson and I.P. Jones, <c+a> dislocations in deformed Ti-6Al-4V micro-cantilevers, Acta Mater. 76 (2014) 127-134.

[30] J. Gong and, A.J. Wilkinson, A microcantilever investigation of size effect, solid-solution strengthening and second-phase strengthening for <a> prism slip in alpha-Ti, Acta Mater. 59 (2011) 5970-5981.

[31] H.A. Khater, A. Serra, R.C. Pond and J.P. Hirth, The disconnection mechanism of coupled migration and shear at grain boundaries, Acta Mater. 60 (2012) 2007-2020.

[32] D.E. Spearot and M.D. Sangid, Insights on slip transmission at grain boundaries from atomistic simulations, Current Opinion in Solid State and Materials Science. 18 (2014) 188-195.

Table Captions

Table 1 The Schmid factors of $\mathbf{a}_1$, $\mathbf{a}_2$ and $\mathbf{a}_3$ for G1 and G2 if the stress axis is assumed simply to be parallel to the LA of the cantilever.

Table 2 Dimensions of slip steps and the corresponding dislocation numbers.

Figure Captions

Figure 1 Schematic illustration of two slip systems intersecting a grain boundary. L are the lines of intersection between the slip plane and grain boundary, n are the plane normals, and the Burgers vector **b** represents the slip direction.

Figure 2 (a) Some microcantilevers across a specific grain boundary (shown by the white line). For G1 a prism plane was about 15° from the sample surface while for G2 a prism plane was nearly parallel to the sample surface. The cantilever long axis is nearly parallel to the basal plane for both grains. (b) A higher magnification SEM image of a micro-cantilever.

Figure 3 (a) Load-displacement data from bend tests on micro-cantilevers cut from the two individual grains G1 and G2 and the G1/G2 bi-crystal. The smooth curves were the result of modelling. (b) crystal plasticity finite element analysis of the bi-crystal showing the distribution near the built-in end of the plastic strain component along the cantilever axis.

Figure 4 (a) An SEM image of a cantilever deflected by 2.8 μm at the load point showing a slip trace on the side of the cantilever and its deviation at the GB (as shown in the inset), (b) an SEM image of a cantilever deflected by 4.0 μm at the load point showing 3 clear slip traces (arrowed) on the top (cantilever) surface of G1 while there are 2 clear slip traces (arrowed) on the G1 cantilever side; there is a slip trace (arrowed) at the bottom of the cantilever for G2. The full white line shows the position at which the TEM foil was cut.

Figure 5 Montages of BF-STEM images from (a) the 2.8 μm deflected sample and (b) the 4.0 μm deflected sample, showing slip bands in both G1 and G2 and the occurrence of slip across the grain boundary (arrowed). The a_1, a_2 and a_3 directions are marked in both G1 and G2. The inset in Fig. 5b was taken from the region containing the neutral line. B.D. ~ [0001].

Figure 6 (a) CBED from G1; (b) CBED from G2 and (c) composite SAD from G1 and G2 (solid line for G2 and dashed line for G1) both nearly along [0001].

Figure 7 Schematic illustration of the slip associated with the grain boundary.
Note: 19° is the angle between $a_3^{(2)}$ and gb facet 1 introduced by slip band 1.

Figure 8 From the 4 μm deflected sample (a) facet 1 (arrowed) is parallel to $(3\bar{2}\bar{1}0)$ referred to G2 (b) facet 3 is not a discrete step: there is a jagged tail.
Note: Figure 8a was taken with the sample tilted until the facet 1 was edge-on. The inset to figure 8a is the corresponding diffraction pattern from G2, which was used to identify the plane of facet 1.

Figure 9 TEM images taken from a region close to the neutral line in Fig. 5b (4 μm deflection). Both images were taken using many beam conditions.

Table 1 The Schmid factors of $\mathbf{a}_1$, $\mathbf{a}_2$ and $\mathbf{a}_3$ for G1 and G2 if the stress axis is assumed simply to be parallel to the LA of the cantilever.

Schmid factors in top grain (G1)	Schmid factors in bottom grain (G2)
0.50 for a_2,	0.47 for a_2,
0.31 for a_3,	0.39 for a_1,
0.19 for a_1	0.10 for a_3

Table 2 Dimensions of slip steps and the corresponding dislocation numbers.

		Slip band # (from left)		
		1	**2**	**3**
Slip step at top of cantilever (corresponding numbers of dislocations)		37 nm (125)	32 nm (108)	35 nm (118)
Incoming dislocations	$a_2^{(1)}$	20	26	32
Reflected dislocations	$a_1^{(1)}$	17	17	27
	$a_3^{(1)}$	19	25	21
Ledge in g.b.	**Length (nm)**	21	23	-
	Plane referred to G2	$(3\bar{2}\bar{1}0)$	$(1\bar{1}00)$	-
Transmitted dislocations	$a_2^{(2)}$	50	36	32
	$a_3^{(2)}$	17	14	18

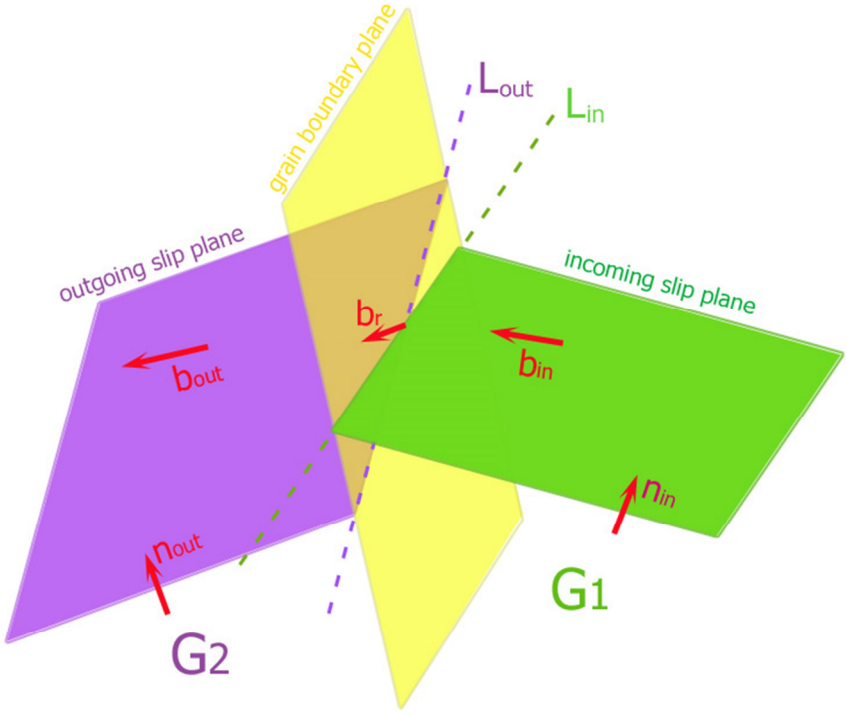

Figure 1 Schematic illustration of two slip systems intersecting a grain boundary. L are the lines of intersection between the slip plane and grain boundary, n are the plane normals, and the Burgers vector **b** represents the slip direction.

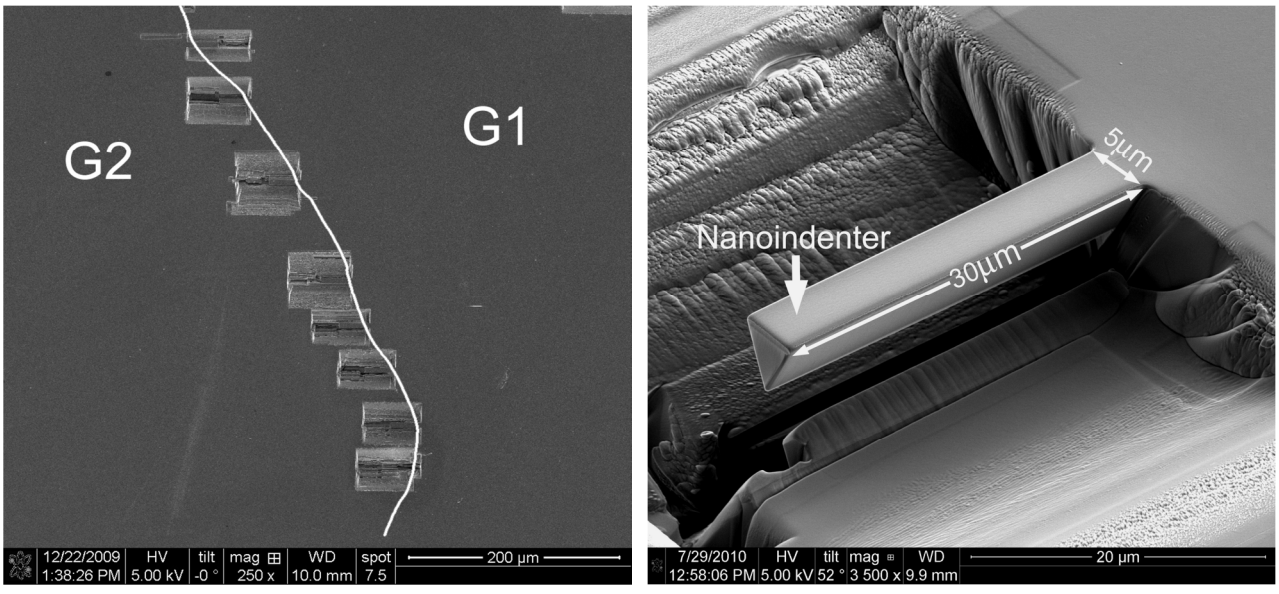

Figure 2 (a) Some microcantilevers across a specific grain boundary (shown by the white line). For G1 a prism plane was about 15° from the sample surface while for G2 a prism plane was nearly parallel to the sample surface. The cantilever long axis is nearly parallel to the basal plane for both grains. (b) A higher magnification SEM image of a micro-cantilever.

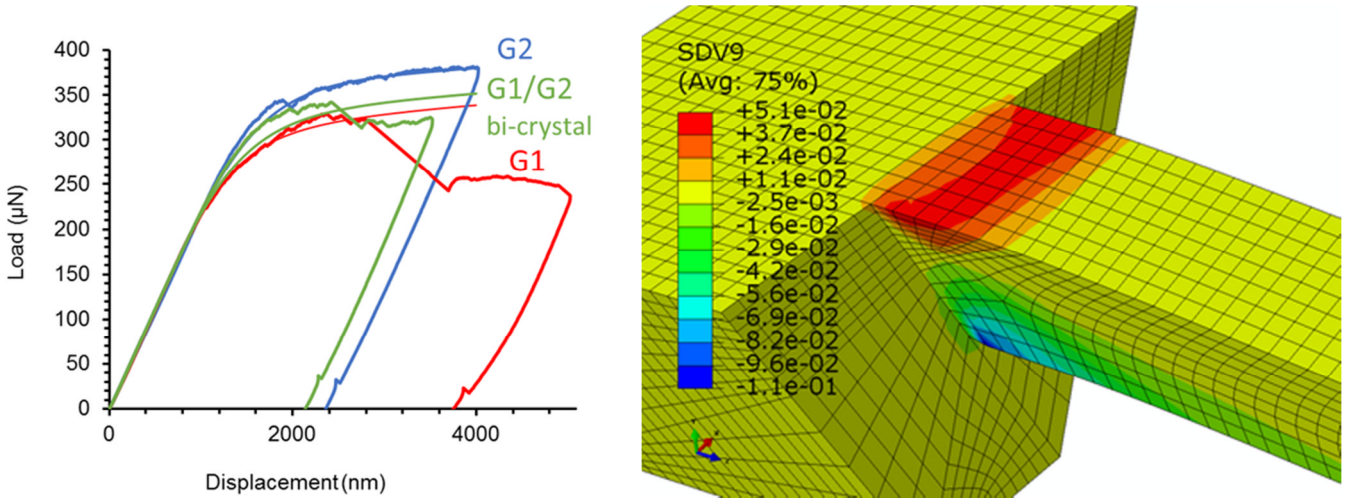

(a) (b)

Figure 3 (a) Load-displacement data from bend tests on micro-cantilevers cut from the two individual grains G1 and G2 and the G1/G2 bi-crystal. The smooth curves were the result of modelling. (b) Crystal plasticity finite element analysis of the bi-crystal showing the distribution near the built-in end of the plastic strain component along the cantilever axis.

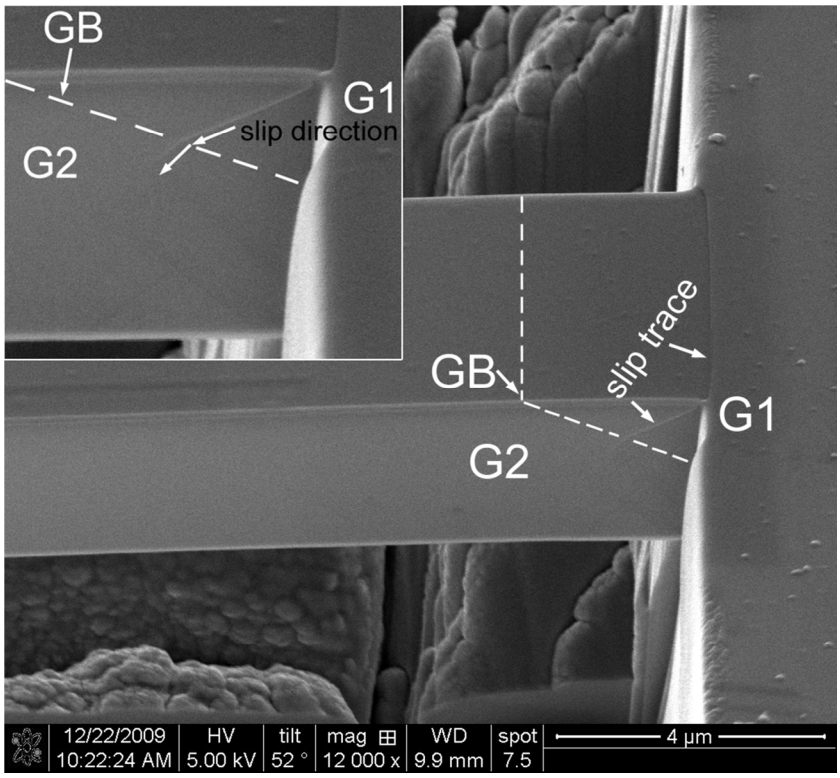

(a)

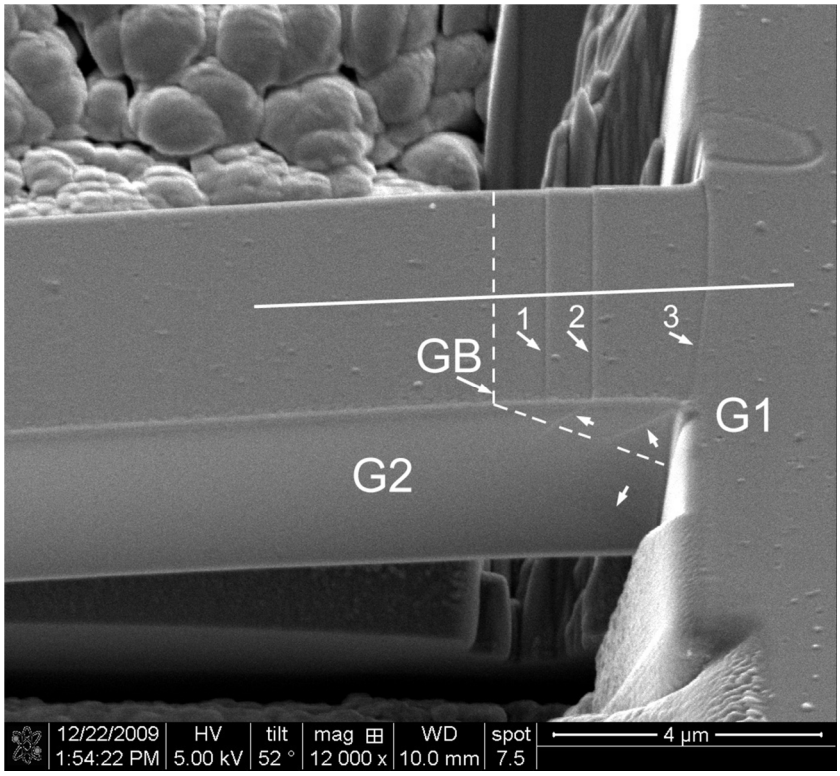

(b)

Figure 4 (a) An SEM image of a cantilever deflected by 2.8 µm at the load point showing a slip trace on the side of the cantilever and its deviation at the GB (as shown in the inset), (b) an SEM image of a cantilever deflected by 4.0 µm at the load point showing 3 clear slip traces (arrowed) on the top (cantilever) surface of G1 while there are 2 clear slip traces (arrowed) on the G1 cantilever side; there is a slip trace (arrowed) at the bottom of the cantilever for G2. The full white line shows the position at which the TEM foil was cut.

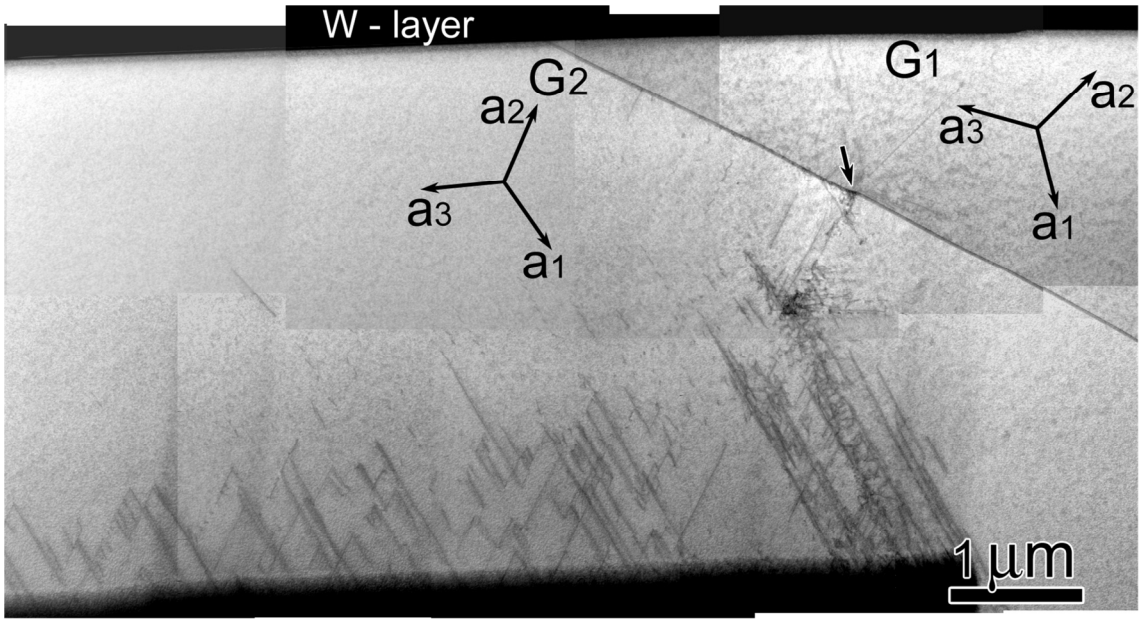

(a)

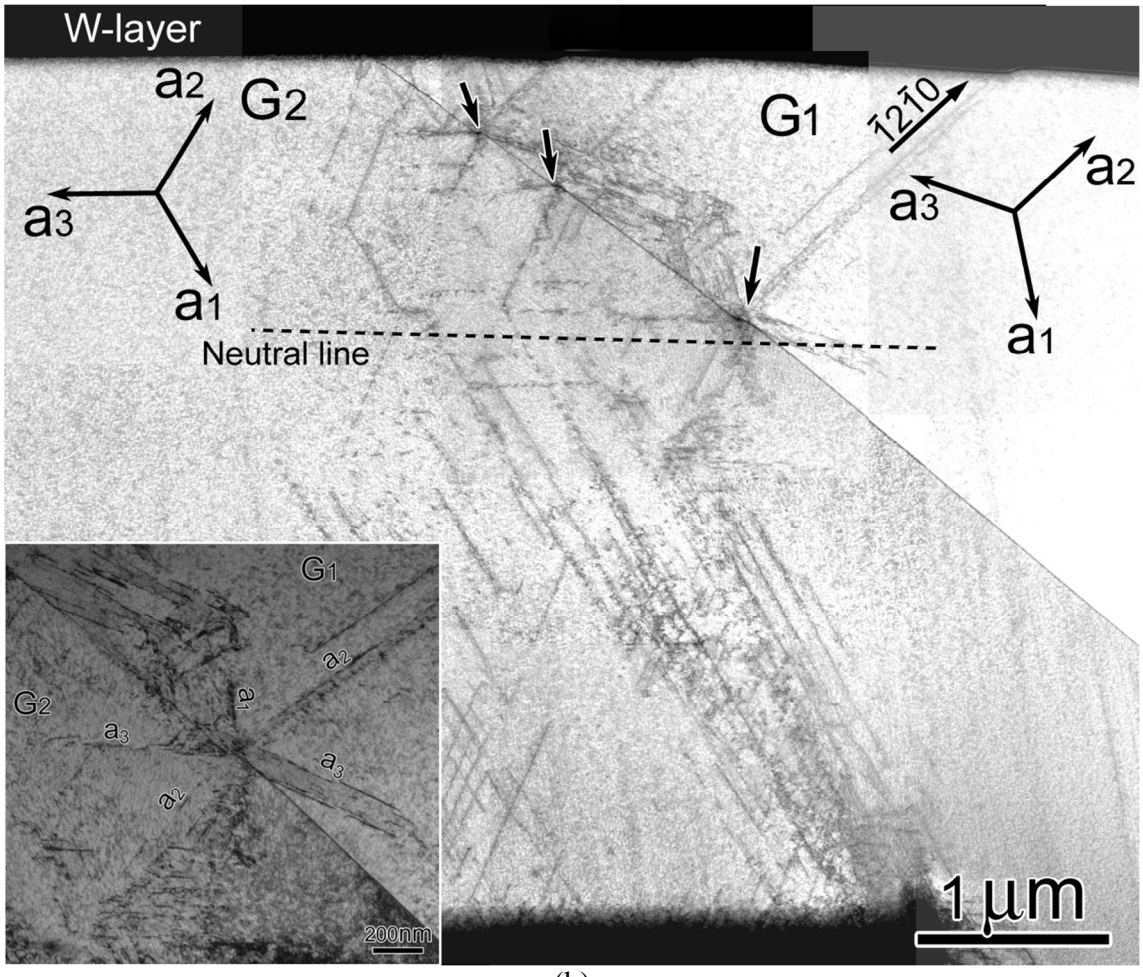

(b)

Figure 5 Montages of BF-STEM images from (a) the 2.8 μm deflected sample and (b) the 4.0 μm deflected sample, showing slip bands in both G1 and G2 and the occurrence of slip across the grain boundary (arrowed). The a_1, a_2 and a_3 directions are marked in both G1 and G2. The inset in Fig. 5b was taken from the region containing the neutral line. B.D. ~ [0001].

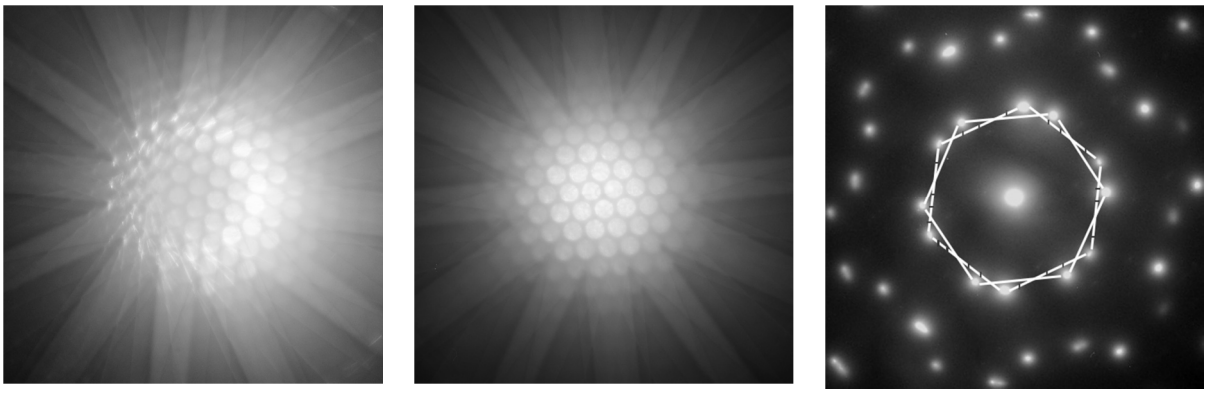

(a) (b) (d)

Figure 6 (a) CBED from G1; (b) CBED from G2 and (c) composite SAD from G1 and G2 (solid line for G2 and dashed line for G1) both nearly along [0001].

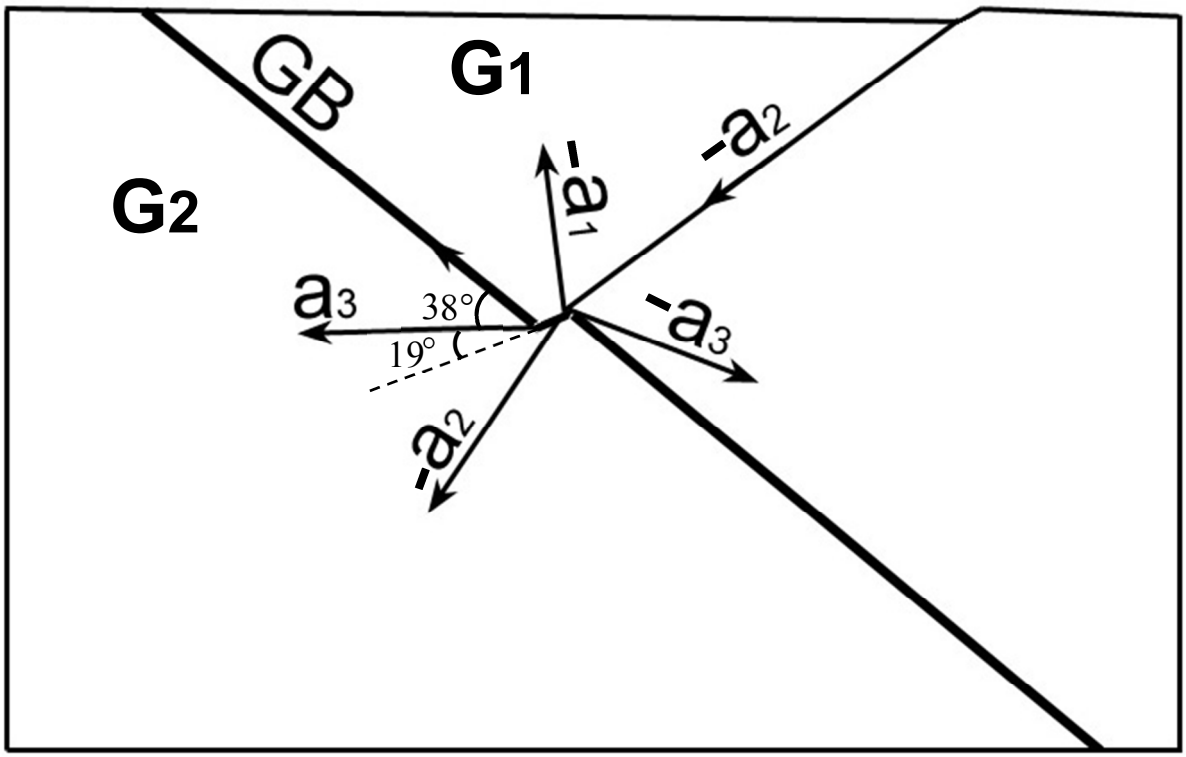

Figure 7 Schematic illustration of the slip associated with the grain boundary.

Note: 19° is the angle between $a_3^{(2)}$ and gb facet 1 introduced by slip band 1.

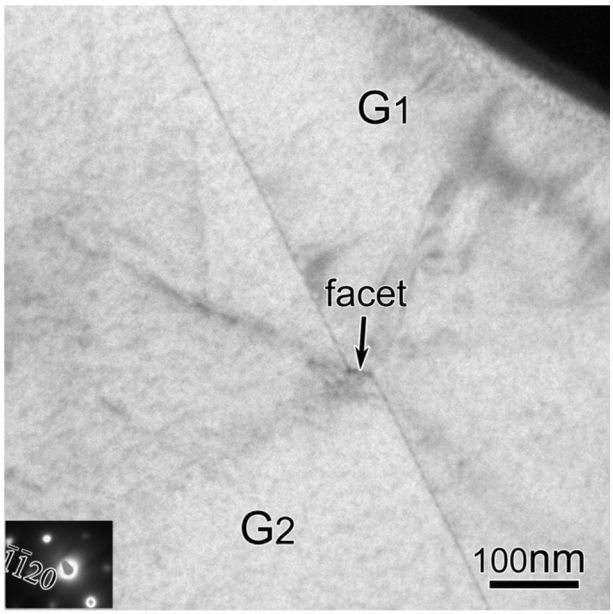

(a)

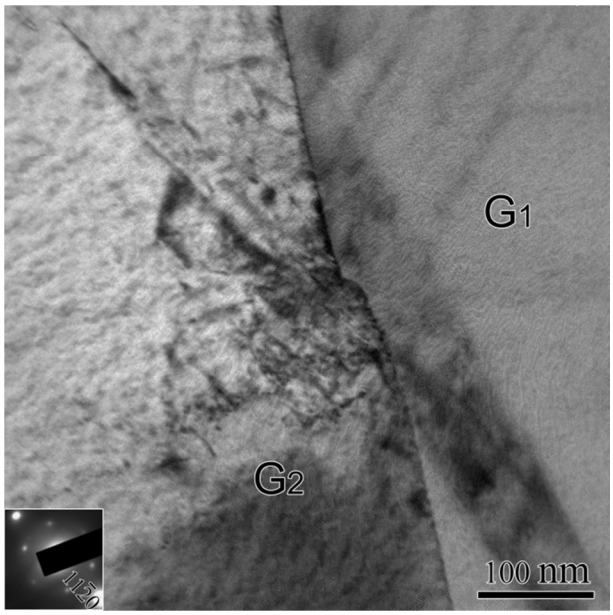

(b)

Figure 8 From the 4 μm deflected sample (a) facet 1 (arrowed) is parallel to $(3\bar{2}\bar{1}0)$ referred to G2 (b) facet 3 is not a discrete step: there is a jagged tail.

Note: Figure 8a was taken with the sample titled until the facet 1 was edge-on. The inset to figure 8a is the corresponding diffraction pattern from G2, which was used to identify the plane of facet 1.

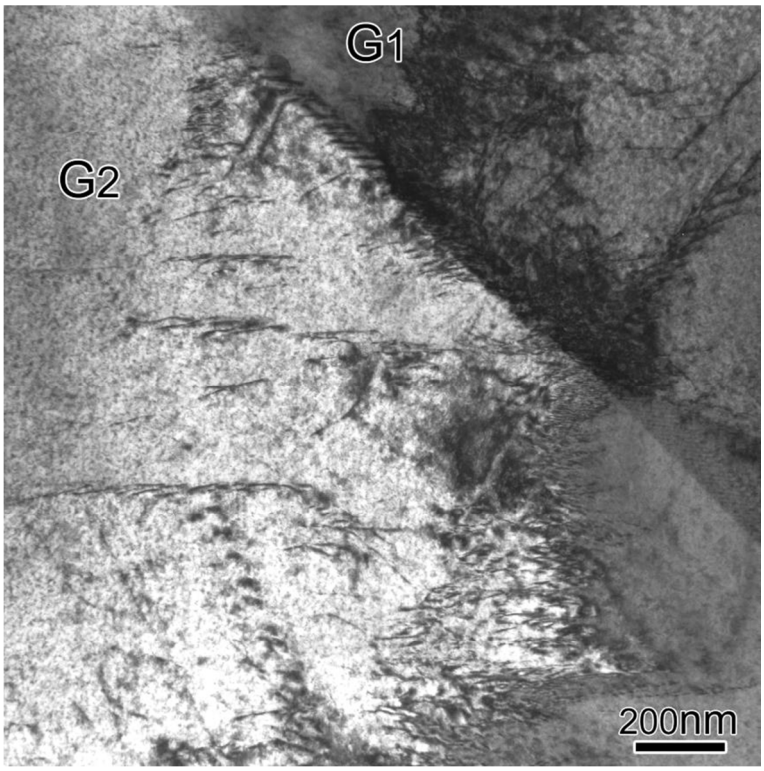

(a)

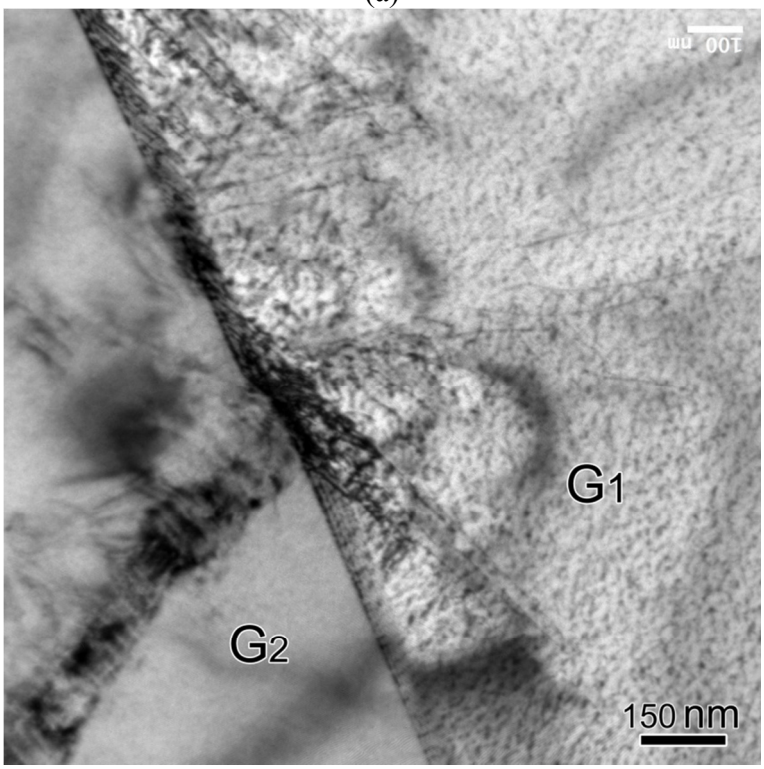

(b)

Figure 9 TEM images taken from a region close to the neutral line in Fig. 5b (4 μm deflection). Both images were taken using many beam conditions.